Materials Chemistry and Physics 296 (2023) 127121

Contents lists available at ScienceDirect

Materials Chemistry and Physics

journal homepage: www.elsevier.com/locate/matchemphys

Multiple equilibria description of type H1 hysteresis in gas sorption isotherms of mesoporous materials

Gion Calzaferri [a,*], Samuel H. Gallagher [b], Simon Lustenberger [b], Fabian Walther [b], Dominik Brühwiler [b,**]

[a] Department of Chemistry, Biochemistry and Pharmaceutical Sciences, University of Bern, Freiestrasse 3, 3012, Bern, Switzerland
[b] Institute of Chemistry and Biotechnology, Zurich University of Applied Sciences (ZHAW), 8820, Wädenswil, Switzerland

HIGHLIGHTS

- Hysteresis in gas sorption isotherms of MCM-41 and of SBA-15 materials is reported.
- Data have been analyzed applying the notion of metastable thermodynamic equilibrium.
- Description provides information on thermodynamic parameters of the H1 hysteresis.
- Values for the enthalpy and the free enthalpy of cavity desorption are obtained.

GRAPHICAL ABSTRACT

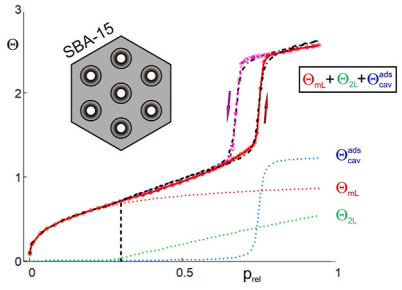

ABSTRACT

We report argon adsorption/desorption isotherms of MCM-41 and of SBA-15. The shape of all hysteresis loops we have observed corresponds to type H1. The data have been analyzed quantitatively using the multiple equilibria description and applying the notion of metastable thermodynamic equilibrium. It is remarkable and important that for both mesoporous materials the desorption process can be understood according to this description but with a corresponding equilibrium constant. This procedure therefore allows determining the thermodynamic values for the enthalpy and the free enthalpy of cavity desorption and thus to obtain information not available so far. We observed that the MCM-41 adsorption isotherms show first an increase with the characteristic Langmuir shape, followed by the almost instantaneous filling of cavities that ends as soon as all cavities are completely filled. The SBA-15 isotherms show a characteristic Langmuir shape at low relative pressure. The pressure slightly below the inflection point at $p_{rel,\ infl} = 0.312$ marks the beginning of the growth of a second layer, before an almost instantaneous filling of cavities takes place. It is interesting to observe that the values of the enthalpy and the free enthalpy for cavity filling and cavity desorption differ by about 0.1 kJ/mol for both, MCM-41 and SBA-15. This means that the driving force for developing a hysteresis is small. The hysteresis loop is therefore driven by delicate changes occurring within the cavities, partially or completely filled by the adsorbate. The monolayer coverage and monolayer desorption processes are decoupled from the cavity filling and cavity emptying processes. Knowing thermodynamic parameters for the hysteresis loop ultimately helps to better characterize and understand the experimental observations.

* Corresponding author.
** Corresponding author.
E-mail addresses: gion.calzaferri@unibe.ch (G. Calzaferri), dominik.bruehwiler@zhaw.ch (D. Brühwiler).
URL: https://calzaferri.dcbp.unibe.ch (G. Calzaferri), http://www.zhaw.ch/icbt/polymer (D. Brühwiler).

https://doi.org/10.1016/j.matchemphys.2022.127121
Received 30 June 2022; Received in revised form 11 October 2022; Accepted 27 November 2022
Available online 15 December 2022

1. Introduction

Argon and nitrogen adsorption isotherms of ordered mesoporous materials such as MCM-41 and SBA-15 are measured under equilibrium conditions. The same applies for the desorption isotherms. The consequence is, that the shape of the adsorption and of the desorption isotherms are expected to be identical within the experimental error. This is, however, not always the case [1–5]. What is the reason? Do we have to assume, that the experimentalist did not meet the equilibrium conditions? It is fair to underline, that most experimental results reported have been carried under the premise that equilibrium was established. The hysteresis loops, however, seem to contradict this assumption. In order to understand this, it is useful to remember the meaning of the term chemical equilibrium condition. We found that hysteresis of type H1 [1] can be interpreted quantitatively based on the multiple equilibria description of adsorption isotherms we have reported previously [6,7], by using the notion of metastable thermodynamic equilibrium [8–10]. The benefit of this is, that thermodynamic parameters for the hysteresis loop can be determined which helps to better characterize and understand the experimental observations. It is useful to first recall some thermodynamic facts to avoid misunderstanding [8,11]. We use the notion of concentrations and not of activities as a simplification without loss of essential insight.

1.1. Direction of a spontaneous chemical reaction

The condition for the direction of a spontaneous chemical reaction can be expressed using the free enthalpy as $dG_{T,p} \leq 0$ or as $\Delta G_{T,p} \leq 0$. This means that in a closed system chemical reactions can proceed at constant temperature T and constant pressure p voluntarily if accompanied by a decrease of free enthalpy. We illustrate this in Fig. 1(A). A spontaneous chemical reaction proceeds in one of the directions indicated by the two arrows, depending on where we start. A stable equilibrium is reached when the change of the free enthalpy is equal to zero, indicated by $dG(\xi)/d\xi = 0$. The equilibrium point is denoted as $\xi = \xi_e$. We consider the reaction A → B under isotherm and isobar conditions. The initial concentrations are $[A]_0$ and $[B]_0$. The symbol ξ stands for the reaction variable, which expresses the change of the concentrations as the reaction proceeds: $[A]=[A]_0 - \xi$ and $[B]=[B]_0 + \xi$. Hence, the reaction quotient Q(ξ) writes as follows:

$$Q(\xi) = \frac{[B]}{[A]} = \frac{[B]_0 + \xi}{[A]_0 - \xi} \tag{1}$$

The free enthalpy change $\Delta G(\xi)$ is expressed as a function of the reaction variable ξ in eqn (2). The equilibrium constant K is related to the free reaction enthalpy $\Delta_R G_0$ as expressed in eqn (3). See SI1 for a derivation of eqn (2).

$$\Delta G(\xi) = -(1-\xi)\Delta_R G_0 + RT[(1-\xi)\ln(1-\xi) + \xi \ln \xi] \tag{2}$$

$$\Delta_R G_0 = -RT\ln K \tag{3}$$

The meaning of eqn (2) is best understood by considering the graph shown in Fig. 1(B). The curve "0" describes the free enthalpy $\Delta G(\xi)$ as a function of the reaction variable ξ not too far away from the equilibrium point A ⇄B indicated by the blue vertical dash-dot line. If at some point the reaction switches such that B′ is formed instead of B according to A → B' the free enthalpy $\Delta G'(\xi)$ path seen as curve "1" is followed instead. The reaction proceeds until the equilibrium point indicated by the black vertical dash-dot line is reached, which means that the local equilibrium A ⇄B′ is established. This local equilibrium, or perhaps better expressed as metastable equilibrium, can be described using the same way as used for describing the stable equilibrium. The condition imposed is that there is a sufficiently high barrier for the conversion B′⟶B which means that the rate of establishing the stable equilibrium is small compared to the rate of establishing the metastable equilibrium so that values of thermodynamic functions are well defined [8–10].

1.2. Model prediction for an MCM-41 type adsorbent

MCM-41 is an ordered mesoporous silicate featuring a hexagonal array of parallel cylindrical pores [12]. The adsorption of nitrogen or argon on MCM-41 begins with the formation of a monolayer on the pristine surface characterized by fractional coverage Θ_{mL}. Sometimes the formation of a second layer Θ_{2L} is seen before an almost instantaneous filling of cavities, denoted by Θ_{cav} [1,13,14], takes place. The adsorption isotherms are therefore described by means of eqn (4), Ref [7].

$$\Theta = \Theta_{mL} + \Theta_{2L} + \Theta_{cav} \tag{4}$$

We show as an example the fractional coverage Θ observed for N_2 adsorption by mesoporous silica MCM-41 [7] in Fig. 2. The theory leading to eqn (5), which describes the cavity filling, bears a formal resemblance to the equilibria formulated for protein interactions with small molecules [15] and hence to an analysis of type IV and type V isotherms recently reported by Buttersack [16]. The parameter n denotes the number of available positions in the cavity, K_{cav} is the equilibrium constant and Θ^0_{cav} is a factor, p_0 denotes the saturation pressure of the adsorptive, R is the ideal gas constant, and T the temperature [7].

$$\Theta_{cav} = \Theta^0_{cav} \frac{\sum_{i=1}^{n} i(p_{rel}k_{cav})^i}{1 + \sum_{i=1}^{n} (p_{rel}k_{cav})^i} \text{ with } k_{cav} = \left(\frac{p_0}{RT}K_{cav}\right) \tag{5}$$

The curves representing the fractional coverage Θ, Θ_{mL}, and

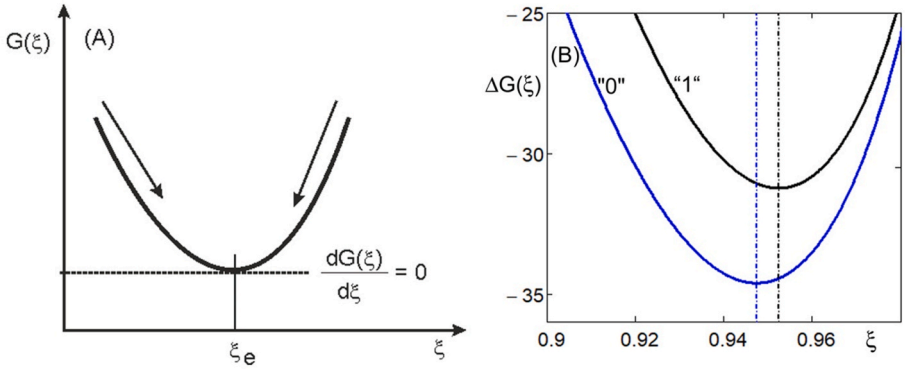

Fig. 1. (A) Free enthalpy G(ξ) as a function of the reaction variable ξ. The equilibrium point is denoted as $\xi = \xi_e$. A spontaneous chemical reaction proceeds in direction of the arrows and a stable equilibrium is reached when the change of the free enthalpy is equal to zero, independent of the direction of the reaction, expressed by $dG(\xi)/d\xi = 0$. (B) Free enthalpy $\Delta G(\xi)$ according to eqn (2) as a function of the reaction variable ξ. The curve "0" describes the reaction A → B while "1" refers to reaction A→ B'. The equilibrium points A ⇄B and A⇄B′, respectively, are indicated by the blue and the black vertical dash-dot lines. The parameters used for calculating the curves "0" and "1" are $K^{(0)} = 20$ and $K^{(1)} = 18$ and the resulting minima are at 31.24 J/K and 34.62 J/K, respectively. (For interpretation of the references to color in this figure legend, the reader is referred to the Web version of this article.)

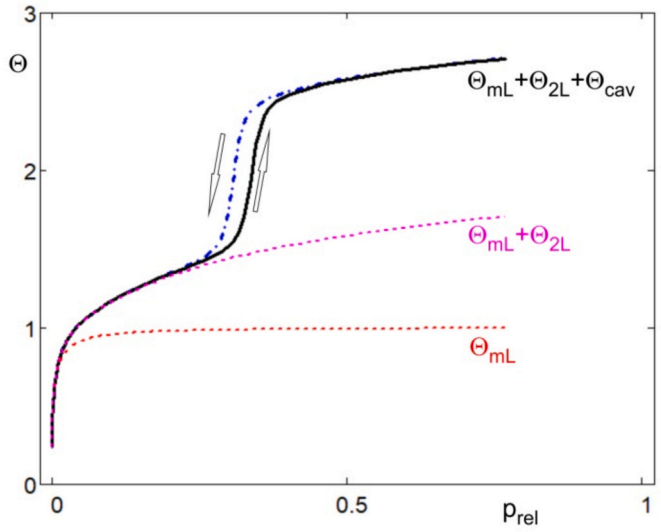

Fig. 2. Nitrogen adsorption isotherm of MCM-41 measured at 77 K, calculated in the range $0 < p_{rel} < 0.8$ and using the parameters reported in Table 4 of ref. [7]. The complete isotherm Θ, shown as black curve, consists of three parts: the monolayer Θ_{mL} evolving on the pristine surface (orange dashed line) and the formation of a second layer Θ_{2L} on top of it. The cavity filling Θ_{cav}, characterized by $K_{cav} = 19.26$ [7], starts before the second layer has been completed. It is shown as part of the solid black curve. The hypothetical H1-type desorption hysteresis, calculated by using $K_{cav}^{des} = 21.21$, is shown as blue dash-dotted line and has purely didactical meaning to illustrate what is formally needed to mimic such a behavior. The adsorption and the hypothetical desorption events are indicated by the upwards and the downwards arrows, respectively. (For interpretation of the references to color in this figure legend, the reader is referred to the Web version of this article.)

$\Theta_{mL}+\Theta_{2L}$ seen in Fig. 2 refer to data observed and were calculated using the parameters reported in Table 4 of Ref [7]. The value for the equilibrium constant K_{cav}, which is of special importance in the present context, amounts to 19.6. The relative pressure for which data are presented is intentionally limited to the range $0 < p_{rel} < 0.8$. If the relative pressure is further increased, the region is reached where other processes such as condensation in interparticle voids take place. It is also the region where minor structural changes, e.g., in the region of cavity openings may occur, which are not detected by the observation of adsorption isotherms, regarding the fact that, e.g., the lowest internal Si–O–Si torsional mode is observed at 40 cm^{-1} and therefore partially activated in the temperature range where adsorption isotherms are measured [17,18]. The system can therefore switch on a slightly different $\Delta G(\xi)$ path as explained in Fig. 1(B). When this happens, the system has in a desorption experiment a chance to follow a new path by establishing at each p_{rel} value a metastable equilibrium with a corresponding value $\Delta_R G_0' = -RT\ln K'$ instead of $\Delta_R G_0 = -RT\ln K$. The consequence is that a hysteresis loop will be observed if the pore diameter is above a critical value, which is determined by the adsorptive and the temperature [19].

1.2.1. Cavity filling

Type H1 hysteresis in open-ended cylindrical pores is often assumed to be caused by the formation of a metastable multilayer film on the pore walls upon adsorption. Desorption, on the other hand, is thought to take place via a receding concave meniscus [5,20,21]. However, experimental evidence seems to suggest that the capillary condensation in cylindrical pores is the equilibrium phase transition, whereas the capillary evaporation is delayed [22,23]. An additional aspect concerns the potential deformation of the pore structure upon capillary condensation [24–26].

We have chosen to use the term cavity filling instead of "capillary condensation" because careful evaluation leads to the result that it is more appropriate in the present context. We are, however, aware of the fact that some authors have been using "capillary condensation" for similar situations. We have therefore added a corresponding remark as Ref. [13], see also Ref. [27].

1.2.2. Model calculation

It is remarkable and important that, as a consequence, desorption can be calculated in the same way as we have reported in Ref. [7] but with a corresponding K_{cav}' value that presents the desorption equilibrium state. This procedure also allows determining the values for $\Delta_{cav}H^{0'}$ and $\Delta_{cav}G^{0'}$ and thus to obtain information not available so far. We cannot distinguish which part of the isotherm, the adsorption or desorption, belongs to the stable and which to the metastable equilibrium. The condition expressed by $dG(\xi)/d\xi = 0$ applies for both, because adsorption and desorption isotherm measurements are designed to represent equilibrium situations.

Θ_{mL} describes the lc2-L (linear combination of 2 Langmuir isotherms) evolution of the monolayer coverage of sites 1 and sites 2 as a function of increasing pressure. It is convenient to use the simplified notations in eqn (6) and (7) for expressing these adsorption equilibria.

$$\{S1\} + X \rightleftarrows \{S1\}X\,,\ KL_1 \tag{6}$$

$$\{S2\} + X \rightleftarrows \{S2\}X\,,\ KL_2 \tag{7}$$

while Θ_{2L} describes the building of a second monolayer on top of the first one.

$$\{\{S1\}X, \{S2\}X\} + X \rightleftarrows \{\{S1\}X, \{S2\}X\}X, K_{2L} \tag{8}$$

The filling of cavities, eqn (9), which is observed to be almost instantaneous and starts before the process (8) is completed, is characterized by Θ_{cav}.

$$\langle\{\{S1\}X, \{S2\}X\}X\rangle X_i + X \rightleftarrows \langle\{\{S1\}X, \{S2\}X\}X\rangle X_{i+1}, K_{cav} \tag{9}$$

We refer to Refs. [6,7] for a detailed discussion of these adsorption processes. Desorption of the second monolayer Θ_{2L} and desorption of the intrinsic monolayer Θ_{mL} are not affected by the emptying of the cavities eqn (10). We have added a dash to the $\langle\{\{S1\}X, \{S2\}X\}X\rangle' X_i$ in order to distinguish the state undergoing desorption.

$$\langle\{\{S1\}X, \{S2\}X\}X\rangle' X_i \rightleftarrows \langle\{\{S1\}X, \{S2\}X\}X\rangle' X_{i-1} + X, K_{cav}^{des} \tag{10}$$

H1 hysteresis is therefore a process that is solely caused by small changes occurring within the cavities, partially or completely filled by adsorbate. This might be exemplified by small contractions supported e.g. by the 40 cm^{-1} torsional Si–O–Si mode [17,18] of the cavity exit which may contribute to delaying the guests until they can escape below a critical pressure. Findenegg et al. studied pore condensation in controlled-pore glass with emphasis regarding the influence of the pore diameter as well as the strength of fluid wall interactions and temperature on the limits of stability and metastability of the adsorbed film [4]. This decoupling of the cavity adsorption/desorption from the monolayer and second monolayer adsorption/desorption can be considered as natural H1 hysteresis isotherm behavior. We compare this description with an experiment we have carried out with an MCM-41 adsorbent at three different temperatures (65 K, 77 K, 87 K) and of SBA-15 (87 K) with argon as adsorptive. An overview of the experimental data is presented in Fig. 3.

2. Experimental

Chemicals. Aqueous ammonia (ACS reagent, 28.0–30.0% NH_3), tetraethyl orthosilicate (TEOS, reagent grade, ≥98%), cetyltrimethylammonium bromide (CTAB, ≥98%), and Pluronic P123 were purchased from Sigma-Aldrich and used without further purification.

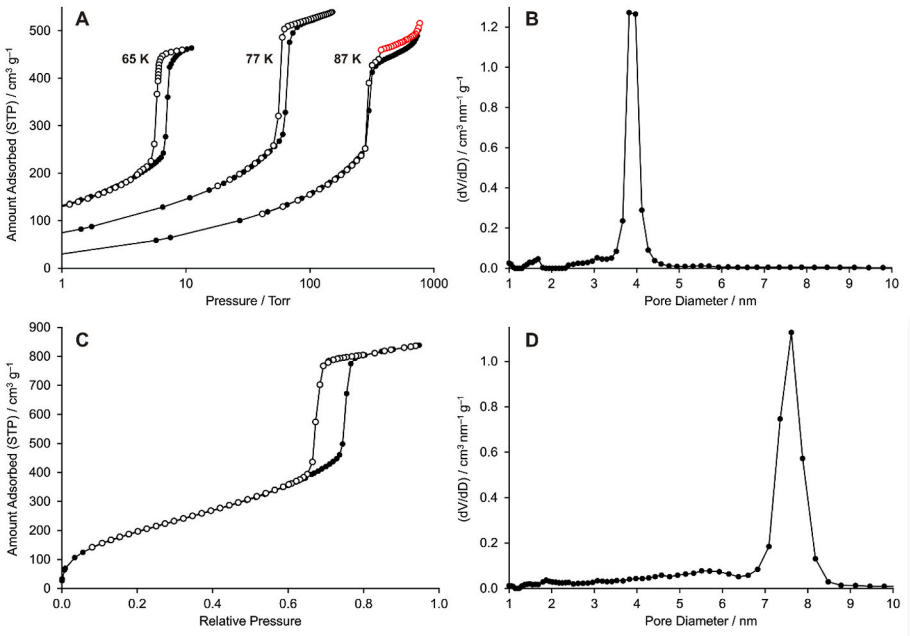

Fig. 3. (A) Argon sorption isotherms of MCM-41 at 65 K, 77 K, and 87 K. Open points denote desorption. The high-pressure hysteresis loop in the measurement at 87 K (red points) is due to condensation in interparticle voids. (B) Pore size distribution of MCM-41 calculated from the 87 K isotherm by means of NLDFT. (C) Argon sorption isotherm of SBA-15 at 87 K. Open points denote desorption. (D) Pore size distribution of SBA-15 calculated by means of NLDFT. See SI2 for a numerical report of the data. (For interpretation of the references to color in this figure legend, the reader is referred to the Web version of this article.)

MCM-41. The synthesis was performed as reported in Ref. [28]. CTAB (2.20 g) was dissolved in a 35 °C solution of 52 mL of water and 25 mL of aqueous ammonia. Once fully dissolved, 10 mL of TEOS was added dropwise under stirring. Stirring was continued for 3 h at room temperature. The mixture was then poured into a Teflon-lined autoclave, which was placed in a preheated oven (110 °C). After 48 h at 110 °C, the autoclave was removed from the oven and allowed to cool to room temperature. The product was filtered and washed with 1 L of water. After allowing the product to dry for some hours the structure-directing agent was removed by calcination (300 °C for 2 h followed by 550 °C for 16 h with a heating rate of 1 °C/min).

SBA-15. The synthesis was performed according to Ref. [29]. P123 (2.20 g) was dissolved in water (49 mL) and HCl (4 M, 31 mL). The mixture was heated to 35 °C and once a clear solution was obtained, TEOS (5 mL) was added dropwise. The mixture was stirred for 20 h at 35 °C. The suspension was then transferred to a Teflon-lined autoclave and placed in a preheated oven set to 100 °C for 24 h. The autoclave was removed and allowed to cool to room temperature. The product was obtained through filtration and washed with 1 L of water. After drying in an oven at 80 °C for 2 h, the structure-directing agent was removed by calcination (550 °C for 5 h at a heating rate of 1 °C/min).

Sorption measurements. Prior to the measurements, the samples were vacuum-degassed at 150 °C for 3 h. The isotherms were measured with a Quantachrome Autosorb iQ MP equipped with a CryoCooler. The saturation vapor pressure p_0 was experimentally determined during the measurements. Pore size distributions were calculated by a nonlocal density functional theory (NLDFT) model developed for silica exhibiting cylindrical pore geometry (software ASiQwin, version 5.0, Quantachrome Instruments).

Data analysis. The Levenberg-Marquardt method [30] implemented in Mathcad [31] was used for the numerical evaluation of the experimental data and to determine the parameters. It is important to first analyze the low relative pressure region, so that the monolayer coverage isotherm Θ_{mL} can be characterized separately. For this, the first experimental inflection point was evaluated. It marks the point p_{infl} where the curvature changes sign and was therefore determined by numerically evaluating the second derivatives which vanish at this point, according to eqn (11), where V_{ads} is the volume adsorbed and p the pressure.

$$\frac{d^2}{dp^2}V_{ads} = 0 \tag{11}$$

The monolayer coverage isotherm Θ_{mL} - see eqn (13) - was determined for the adsorption isotherm range $p \leq \frac{3}{4}p_{infl}$ or $p_{rel} \leq \frac{3}{4}p_{rel,infl}$, respectively, to make sure that the contribution of the next adsorption process remains negligibly small. In the next step the cavity filling Θ_{cav} step was analyzed, eqn (14) or eqn (16). The residuals shown in Figs. 4 and 5 are the difference between the experimental and the calculated values, [6,7].

3. Results and discussion

The isotherm data shown in Fig. 3 have been analyzed using results reported in Refs. [6,7] in the manner we have explained in the discussion of Fig. 2. All adsorption isotherms show first an increase with the characteristic Langmuir shape, sometimes decorated by the growth of an additional layer, followed by the almost instantaneous filling of cavities that ends as soon as all cavities are completely filled. The volume available in the cavities defines the upper limit of the process. We first discuss the adsorption/desorption isotherms of MCM-41.

3.1. MCM-41

Fig. 3(A) shows that a reversible type IV(b) isotherm is obtained at 87 K. Lowering the temperature leads to IV(a) isotherms. The opening of the hysteresis loop at decreasing temperature can be exploited to obtain information about the pore connectivity. In fact, argon adsorption at 77 K has for this reason been suggested as a viable alternative to the much more common nitrogen adsorption at 77 K. Hysteresis in cylindrical pores can be observed for a larger range of pore sizes when using argon instead of nitrogen as an adsorptive at 77 K [32]. As expected, MCM-41 features a type H1 hysteresis, indicating the absence of network effects in the adsorption/desorption process. The adsorption isotherm in terms of fractional coverage Θ_{ads} can be expressed by means of eqn (12), because we observed no indication for the formation of a second monolayer on top of the first one. The symbol Θ_{mL} describes the formation of the monolayer evolving on the pristine surface and the symbol Θ_{cav}^{ads} stands for the cavity filling.

$$\Theta_{ads} = \Theta_{mL} + \Theta_{cav}^{ads} \tag{12}$$

Analysis of the data leads to the result that Θ_{mL} must be expressed as a sum of two Langmuir isotherms, eqn (13), which follows from what we

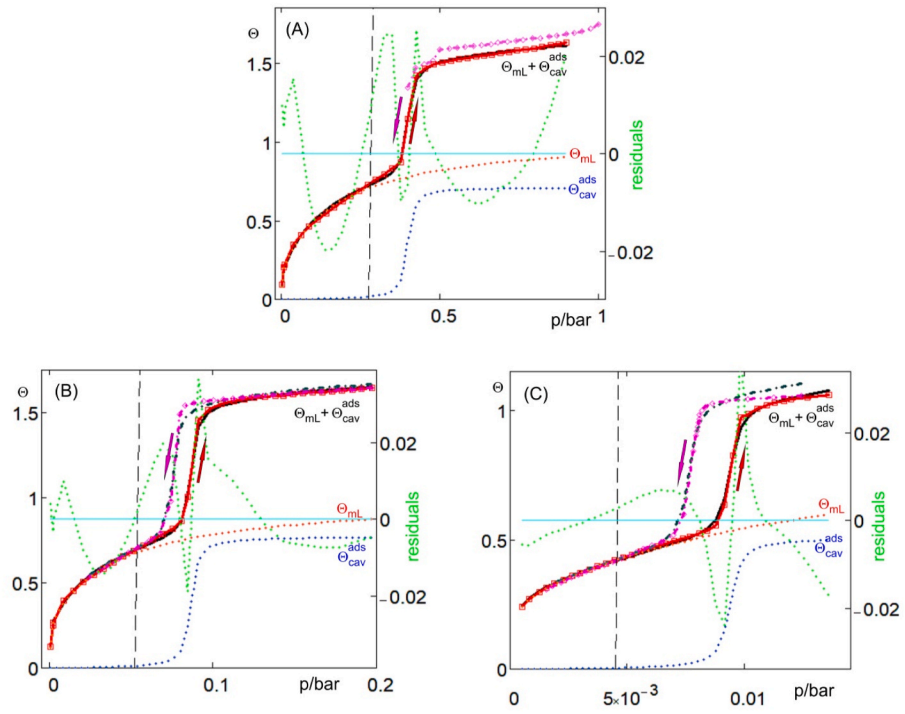

Fig. 4. Analysis of the argon adsorption/desorption isotherms of MCM-41 at (A) 87 K, (B) 77 K, and (C) 65 K, reported in Fig. 3(A). The fractional coverage Θ is plotted versus the pressure p in bar. The arrows indicate the direction of the adsorption (red) and the direction of the desorption (violet). The experimental data of the adsorption are shown as red circles connected with a red solid line and the calculation as black solid line. The experimental desorption data are shown as violet circles connected with a violet dash-dot line. The result of the calculation is shown as black dash-dot line. The residuals which represent the difference between the experimental data and the calculation, shown for the adsorption isotherms, are drawn as green dotted lines. We also show the contribution of the Langmuir Θ_{mL} as red dotted line and the contribution of the cavity filling Θ_{cav}^{ads} as blue dotted line. The position of the first experimental inflection point is shown as black vertical dashed line. (For interpretation of the references to color in this figure legend, the reader is referred to the Web version of this article.)

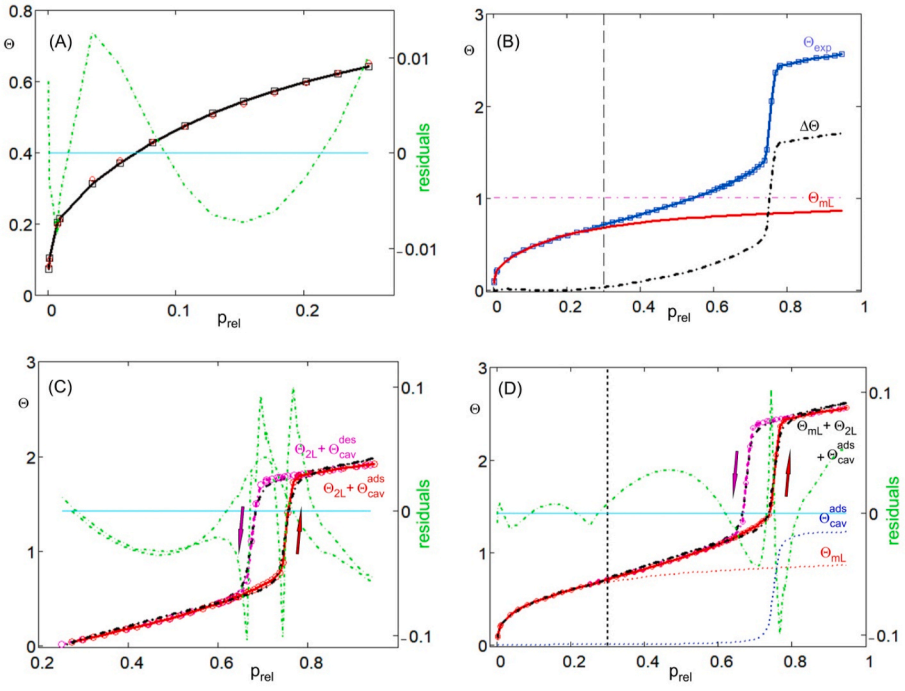

Fig. 5. Analysis of the argon adsorption/desorption isotherms of SBA-15, Fig. 3(C and D). The fractional coverage Θ is plotted versus the relative pressure p_{rel}. (A) Description of the data in the relative pressure range $0 \leq \frac{3}{4}p_{rel,infl}$ by means of the lc2-L eqn (13). The experimental data are shown as red circles connected with a red solid line. The result of the calculation is shown as black solid line and black squares. The residuals which represent the difference between the experimental data and the calculation are drawn as green dotted line. (B) The experimental data Θ_{exp} are shown as blue circles connected with a blue solid line. The position of the first experimental inflection point is shown as black vertical dashed line. The red solid line indicates the Langmuir isotherm Θ_{mL}, and the dash-dot dot line shows the difference $\Delta\Theta = \Theta_{exp}$-$\Theta_{mL}$ (ref [7], eqn (3)). (C) Numerical description of the difference ΔΘ by means of $\Theta_{2L} + \Theta_{cav}$ and $\Theta_{2L} + \Theta_{cav}^{des}$ for the adsorption and desorption, respectively. The experimental data of the adsorption are shown as red circles connected with a red solid line and those of the desorption are shown as violet circles connected with a violet dash-dot line. The arrows indicate the direction of the adsorption (red) and the direction of the desorption (violet). The result of the calculation is shown as black dash-dot line. The residuals are shown as green dotted lines. (D) Description of the whole argon adsorption/desorption isotherms. The colors are used as in (C). The residuals refer to the adsorption; those for desorption look nearly the same; see (C). We also show the contribution of the Langmuir Θ_{mL} as red dotted line and the contribution of the cavity filling Θ_{cav}^{ads} as blue dotted line. The position of the first experimental inflection point is shown as black vertical dashed line. (For interpretation of the references to color in this figure legend, the reader is referred to the Web version of this article.)

have observed previously for several types of adsorbents [6]. The description of the low pressure part as sum of Langmuir isotherms has been used for analyzing systems consisting of several sites with different ease of adsorption and for multicomponent gas analysis [33–38]. This type of description is reasonable given the heterogeneity of the silica surface [39]. We have extended the analysis of multiple equilibria of compounds with different coordination sites [40] to the explanation of adsorption isotherms for adsorbents bearing different sites, focusing on

the low pressure range, i.e., on conditions where the adsorptive-adsorbent binding strength is larger than the adsorptive-adsorbate, so that monolayer coverage is favored [6]. The derivation of eqn. (14), which describes the sudden filling of the cavities, has been discussed in detail in Ref. [7].

$$\Theta_{mL} = \frac{1}{V_{mL}}\left[a_1\frac{KL_1p'}{1+KL_1p'} + a_2\frac{KL_2p'}{1+KL_2p'}\right] \quad (13)$$

$$\Theta_{cav}^{ads} = \frac{1}{V_{mL}}\left[a_{cav}\frac{\sum_{i=1}^{n} i(p'k_{cav}RT)^i}{1+\sum_{i=1}^{n}(p'k_{cav}RT)^i}\right] \text{ with } k_{cav} = K_{cav}\frac{p^{\varnothing}}{RT} \quad (14)$$

In these equations p' is the pressure divided by the pressure unit $p^{\varnothing}$, KL_1 and KL_2 denote the Langmuir constants and the parameters a_1 and a_2 express the amount of adsorptive adsorbed on sites 1 and on sites 2, respectively, while the monolayer coverage volume V_{mL} is equal to $a_1 + a_2$. K_{cav} is the equilibrium constant for cavity filling, a_{cav} denotes the amount which is to some extent correlated to the lower limit of available sites n in a cavity. The value of n is chosen to be 100 [41]. R denotes the ideal gas constant and T the temperature. The desorption isotherm Θ_{des} differs from eqn (12) only in the second term because the monolayer desorption shows no hysteresis:

$$\Theta_{des} = \Theta_{mL} + \Theta_{cav}^{des} \quad (15)$$

This means, that in eqn (14) a_{cav} and K_{cav} are replaced by a_{cav}^{des} and K_{cav}^{des}, respectively. The results of this interpretation are collected in Fig. 4 and Table 1.

The results depicted in Fig. 4 illustrate that the experimental results can be quantitatively interpreted based on eqns (12) and (15). The resulting parameters are collected in Table 1. There is no surprise that all adsorption isotherms can be described very well by means of eqn (12). The new data are an additional support of the results reported in Refs. [6,7]. The new aspect concerns the analysis of the hysteresis seen for the isotherms at 77 K and 65 K. We observe that the shift of the cavity desorption with respect to the adsorption can be described independently from the monolayer Langmuir Θ_{mL} coverage. It is instructive to observe the Θ_{mL} and the Θ_{cav}^{ads} contributions separately, as shown in Fig. 4. The difference of Θ_{cav}^{des} with respect to Θ_{cav}^{ads} is apart from the shift so small that we do not show it separately. The values of the enthalpy and the free enthalpy for adsorption measured at 87 K are similar to those previously obtained for MCM-41 with a slightly larger pore diameter [7]. The same applies for the cavity filling parameters. It is not unexpected to observe that the enthalpy and the free enthalpy for monolayer adsorption show little change with temperature, while the Langmuir constants KL_1 and KL_2 as well as K_{cav} show the expected increase with decreasing temperature. We remind that all numerical values $\Delta_{ads}H_i^{\varnothing}$, $\Delta_{cav}H^{\varnothing}$, and $\Delta_{cav}^{des}H^{\varnothing}$ are larger than the enthalpy of vaporization of argon which amounts to $\Delta_{vap}H^{\varnothing}(Ar, 87K) = 6.5$ kJ/mol [42]. It is interesting to observe that the values of the enthalpy and the free enthalpy for cavity filling and cavity desorption differ by only about 0.1 kJ/mol. This means that the driving force for developing a hysteresis is very small, even smaller than the energy of a 40 cm^{-1} torsional Si–O–Si mode (which amounts to 0.48 kJ/mol). The shift to larger fractional coverage of the desorption curve above p = 0.5 bar of the measurement at 87 K, Fig. 4(A), with respect to the adsorption isotherm could be connected to the fact that data were measured up to 1.025 bar. It is very likely that interparticle condensation takes place so close at the argon saturation pressure of 1.069 bar. We do not attempt to describe this process quantitatively. We therefore analyze only the adsorption isotherm up to p = 0.9 bar and no desorption parameters are reported in Table 1.

3.2. SBA-15

Compared to MCM-41 the pore structure of SBA-15 is more complex. Several studies have shown that in addition to the well-defined primary mesopores, the SBA-15 structure features a broad range of secondary mesopores and micropores, which can form bridges between the primary mesopores [43–46]. The pore size distribution depicted in Fig. 3 (D) indeed shows a minor contribution of secondary mesopores and supermicropores. The argon sorption isotherm of SBA-15 is of type IV(a) with a pronounced H1 hysteresis. We have analyzed the isotherm in the same way as described above. The first step is to derive the first inflection point, which was found to be $p_{rel,\,infl} = 0.312$. This allows to sort out the low pressure range $p_{rel} \leq \frac{3}{4}p_{rel,infl}$. We illustrate in Fig. 5(A) that the lc2-L eqn (13) describes the low pressure data perfectly well, similar as we have already observed for several different adsorbents reported in Ref. [6]. The resulting data are reported in Table 1. We observe that they are within the range of the MCM-41 data at 87 K. Deducing the Langmuir monolayer formation isotherm Θ_{mL} from the experimental data according $\Delta\Theta = \Theta_{exp} - \Theta_{mL}$ seen in Fig. 5(B), as we have discussed in Ref. [7] eqn (3), indicates clearly the formation of a second layer Θ_{2L} before an almost instantaneous filling of cavities takes place. This difference can be analyzed separately, the same as for the MCM-41 data shown in Fig. 4 and discussed in Ref. [7]. We illustrate this in Fig. 5(C) where we compare the numerical description of the difference $\Delta\Theta$ by means of $\Theta_{2L} + \Theta_{cav}$ and $\Theta_{2L} + \Theta_{cav}^{des}$ for the adsorption and desorption, respectively. This means that eqn (4) applies for the description of the full adsorption isotherms, and correspondingly eqn (16) holds for the description of the desorption.

$$\Theta_{des} = \Theta_{mL} + \Theta_{2L} + \Theta_{cav}^{des} \quad (16)$$

We show the result of this description in Fig. 5(D) and in Table 1. It

Table 1
Parameters for the MCM-41 and SBA-15 isotherms.

Temp [K] adsorbent	i	a_i [cm^3/g]	KL_i	$\Delta_{ads}G_i^{\varnothing}$/ $\Delta_{ads}H_i^{\varnothing}$ [kJ/mol]	$V_{m,Lm}$ [cm^3/g]	A_{Lm} [m^2/g]	a_{cav} [cm^3/g]	K_{cav}	$\Delta_{cav}G^{\varnothing}$/ $\Delta_{cav}H^{\varnothing}$ [kJ/mol]	a_{cav}^{des} [cm^3/g]	K_{cav}^{des}	$\Delta_{cav}^{des}G^{\varnothing}/\Delta_{cav}^{des}H^{\varnothing}$ [kJ/mol]
87	1	58	575	-4.6/11.1	300	1100	2.1	18	−2.1/-8.6	–	–	–
MCM-41[a)]	2	246	5.4	-1.2/-7.7								
77	1	85	2950	-5.1/-11.0	330	1250	2.5	74	−2.7/-8.5	2.6	85	−2.8/-8.6
MCM-41[b)]	2	246	24	-2.0/-7.8								
65	1	119	8360	-4.9/-9.7	380	1450	2.2	575	−3.4/-8.3	2.4	708	−3.5/-8.4
MCM-41[c)]	2	61	73	-2.3/-7.2								
87	1	67	845	-4.9/-11.4	327	1250	1.78	9	−1.6/-8.1	1.76	10	−1.7/-8.2
SBA-15[d)]	2	261	4.6	-1.1/-7.6								

a) $p_{infl} = 0.286$ bar.
b) $p_{infl} = 0.053$ bar.
c) $p_{infl} = 4.46 \times 10^{-3}$ bar.
d) Results of the argon SBA-15 isotherms measured at 87 K using eqn (12) for the adsorption and eqn (15) for the desorption isotherms ($i_{cav} = 235$); both extended by Θ_{2L} according to eqn (4). $a_{2L} = 1600$, $K_{2L} = 0.87$, $\Delta_{ads}G_{2L}^{\varnothing} = 0.1$ kJ/mol, $\Delta_{ads}H_{2L}^{\varnothing} = -6.7$ kJ/mol, $p_{rel,\,infl} = 0.312$.

fully supports the reasoning presented. It is interesting that the parameter $i_{cav} = 235$, which is related to the free volume of the cavity, is significantly larger than the value for the MCM-41. It corresponds to the volume of a cylinder of 2.4 nm length and diameter, that the size of the cavities is at least as large but can also be larger. It appears that the i_{cav} parameters reflect the different pore diameters of MCM-41 (3.9 nm) and of SBA-15 (7.6 nm). It is therefore not surprising that the values for the free enthalpy $\Delta_{cav}G^{\varnothing}$ and the enthalpy $\Delta_{cav}H^{\varnothing}$ for cavity filling are smaller than those for the MCM-41 measured at the same temperature. We observe again that all numerical values $\Delta_{ads}H_i^{\varnothing}$, $\Delta_{cav}H^{\varnothing}$, and $\Delta_{cav}^{des}H^{\varnothing}$ are larger than the enthalpy of vaporization of argon. The value measured for the second monolayer formation $\Delta_{ads}H_{2L}^{\varnothing}$, however, is nearly the same or even slightly smaller. This explains why only a small part of the second monolayer formation is realized before cavity filling occurs. Again, we observe that the values of the enthalpy and the free enthalpy for cavity filling and cavity desorption differ by only about 0.1 kJ/mol. This means that the driving force for developing a hysteresis is small, even smaller than, e.g., the energy of a 40 cm^{-1} torsional Si–O–Si mode.

4. Conclusions

We report argon adsorption/desorption isotherms of MCM-41 measured at 87 K, 77 K, and 65 K and of SBA-15 measured at 87 K. The data have been analyzed using the multiple equilibria description and procedures reported previously [6,7], and applying the notion of metastable thermodynamic equilibrium. We observed that the MCM-41 adsorption isotherms show first an increase with the characteristic Langmuir shape, followed by the almost instantaneous filling of cavities that ends as soon as all cavities are completely filled. The volume available in the cavities defines the upper limit of the process. The SBA-15 isotherms show characteristic Langmuir shape at low relative pressure. The pressure slightly below the inflection point at $p_{rel,\ infl} = 0.312$ marks the beginning of the growth of a second layer, before an almost instantaneous filling of cavities takes place. The shape of all hysteresis loops we have investigated corresponds to type H1 [1]. It is remarkable and important that for both the MCM-41 and SBA-15 the desorption process can be understood in the same way as we have reported in Ref. [7] but with a corresponding K'_{cav} value that presents the cavity desorption equilibrium state. This procedure therefore allows determining the values for $\Delta_{cav}H^{0'}$ and $\Delta_{cav}G^{0'}$ and thus to obtain information not available so far. This further underlines the validity of the theoretical concept. All numerical values $\Delta_{ads}H_i^{\varnothing}$, $\Delta_{cav}H^{\varnothing}$, and $\Delta_{cav}^{des}H^{\varnothing}$ are larger than the enthalpy of vaporization of argon which amounts to $\Delta_{vap}H^{\varnothing}(Ar, 87K) = 6.5$ kJ/mol [42]. It is interesting to observe that the values of the enthalpy and the free enthalpy for cavity filling and cavity desorption differ only by about 0.1 kJ/mol for both, MCA-41 and SBA-15. This means that the driving force for developing a hysteresis is very small. The hysteresis loop is therefore driven by minor changes occurring within the cavities, partially or completely filled by the adsorbate. We cannot distinguish which part of the isotherm, the adsorption or desorption, belongs to the stable and which to the metastable equilibrium. The condition expressed by $dG(\xi)/d\xi = 0$ applies for both, because adsorption and desorption isotherm measurements are designed to represent equilibrium situations. It turns out, however, that the monolayer coverage and monolayer desorption processes are decoupled from the cavity filling and cavity emptying processes. The emptying is symmetrical with the cavity filling process and described by the same but reversed process. The atomistic processes causing the delayed release cannot be fully elucidated by measuring adsorption/-desorption isotherms without monitoring additional information. Monitoring vibrational modes in the low frequency range reflecting the small energy difference separating the two processes could lead to further atomistic insight. In summary, hysteresis of type H1 can be interpreted quantitatively based on the multiple equilibria description of adsorption isotherms we have reported previously [6,7], by using the notion of metastable thermodynamic equilibrium [8,9]. The benefit of this is, that thermodynamic parameters for the hysteresis loop can be determined which helps to better characterize and understand the experimental observations.

CRediT authorship contribution statement

Gion Calzaferri: Conceptualization, Theory, Formal analysis, Software, Validation, Visualization, Writing – review & editing. **Samuel H. Gallagher:** Investigation, Data curation, Formal analysis, Visualization. **Simon Lustenberger:** Investigation, Validation, Data curation, Formal analysis, Writing – review & editing. **Fabian Walther:** Investigation, Validation, Data curation, Formal analysis, Writing – review & editing. **Dominik Brühwiler:** Conceptualization, Funding acquisition, Project administration, Supervision, Validation, Visualization, Writing – review & editing.

Declaration of competing interest

The authors declare that they have no known competing financial interests or personal relationships that could have appeared to influence the work reported in this paper.

Data availability

Experimental isotherm data are given in the SI.

Acknowledgements

This work was supported by the Swiss National Science Foundation (project 200021_172805)

Appendix A. Supplementary data

Supplementary data to this article can be found online at https://doi.org/10.1016/j.matchemphys.2022.127121.

References

[1] M. Thommes, K. Kaneko, A.V. Neimark, J.P. Olivier, F. Rodriguez-Reinoso, J. Rouquerol, K.S.W. Sing, Pure Appl. Chem. 87 (2015) 1051–1069.
[2] M. Thommes, R. Köhn, M. Fröba, Appl. Surf. Sci. 196 (2002) 239–249.
[3] N. Speil, F. Hoffmann, F.J. Brieler, M. Fröba, Microporous Mesoporous Mater. 328 (2021), 111442.
[4] G.H. Findenegg, S. Gross, Th Michalski, In characterization of porous solids III, in: J. Rouquerol, F. Rodriguez-Reinoso, K.S.W. Sing, K.K. Unger (Eds.), Stud. Surf. Sci. Catal. 87 (1994) 71–80.
[5] A. Papadopoulou, F. van Swol, U. Marini Bettolo Marconi, J. Chem. Phys. 97 (1992) 6942–6952.
[6] G. Calzaferri, S.H. Gallagher, D. Brühwiler, Microporous Mesoporous Mater. 312 (2021), 110744.
[7] G. Calzaferri, S.H. Gallagher, D. Brühwiler, Microporous Mesoporous Mater. 330 (2022), 111563.
[8] R.S. Berry, S.A. Rice, J. Ross, Physical Chemistry, Chapters 19 and 20, John Wiley & Sons, NY, 1980, ISBN 0-471-04829-1.
[9] A. Katchalsky, P.F. Curran, Nonequilibrium Thermodynamics in Biophysics, Harvard Univ. Press, Cambridge MA, 1967 (Chapter 7), Library of Congress Catalog Card Number 65-22045.
[10] a)A system ist in a state of Stable Equilibrium if, after Displacement to a New State and Release of the Constraints Causing the Displacement, it Always Returns to the Original State;.
b)A System Is in a State of Metastable Equilibrium if Displacements to Nearby States Satisfy Condition a), but after Displacements to Distant States it Does Not Return to the Metastable State.
[11] K. Denbigh, The Principles of Chemical Equilibrium, second ed., Cambridge University Press, 1966.
[12] a) C.T. Kresge, M.E. Leonowicz, W.J. Roth, J.C. Vartuli, J.S. Beck, Nature 359 (1992) 710–712;
b) J.S. Beck, J.C. Vartuli, W.J. Roth, M.E. Leonowicz, C.T. Kresge, K.D. Schmitt, C. T.-W. Chu, D.H. Olson, E.W. Sheppard, S.B. McCullen, J.B. Higgins, J.L. Schlenker, J. Am. Chem. Soc. 114 (1992) 10834–10843.

[13] Cavity filling is often referred to as capillary condensation, however, we prefer using the more specific term “cavity filling” within the present context; despite of the cylindrical channel type structure of the adsorbents discussed.
[14] a) R. Atluri, Z. Bacsik, N. Hedin, A.E. Garcia-Bennett, Microporous Mesoporous Mater. 133 (2010) 27–35;
b) C. Bernal, M. Mesa, M. Jaber, J.L. Guth, L. Sierra, Microporous Mesoporous Mater. 153 (2012) 217–226.
[15] I.M. Klotz, Acc. Chem. Res. 7 (1974) 162–168.
[16] a) C. Buttersack, Phys. Chem. Chem. Phys. 21 (2019) 5614–5626;
b) C. Buttersack, Microporous Mesoporous Mater. 316 (2021), 110909.
[17] C. Marcolli, P. Lainé, R. Bühler, G. Calzaferri, J. Tomkinson, J. Phys. Chem. B 101 (1997) 1171–1179.
[18] U. Buchenau, M. Prager, N. Nücker, A.J. Dianoux, N. Ahmad, W.A. Phillips, Phys. Rev. B 34 (1986) 5665–5673.
[19] C.G. Sonwane, P.J. Ludovice, J. Mol. Catal. Chem. 238 (2005) 135–137.
[20] P.A. Monson, Microporous Mesoporous Mater. 160 (2012) 47–66.
[21] B. Coasne, A. Galarneau, F. Di Renzo, R.J.M. Pellenq, Langmuir 26 (2010) 10872–10881.
[22] a) E.A. Ustinov, D.D. Do, M. Jaroniec, J. Phys. Chem. B 109 (2005) 1947–1958;
b) E.A. Ustinov, Langmuir 24 (2008) 6668–6675.
[23] M. Kruk, M. Jaroniec, J. Phys. Chem. B 106 (2002) 4732–4739.
[24] A.K. Soper, D.T. Brown, J. Chem. Phys. 154 (2021), 184503.
[25] P.-A. Albouy, A. Ayral, Chem. Mater. 14 (2002) 3391–3397.
[26] C. Balzer, A.M. Wang, S. Gehret, G. Reichenauer, F. Putz, N. Hüsing, O. Paris, N. Bernstein, G.Y. Gor, A.V. Neimark, Langmuir 33 (2017) 5592–5602.
[27] D.H. Everett, Manual of symbols and terminology for physicochemical quantities and units, appendix II: definitions, terminology and symbols in colloid and surface chemistry, Pure Appl. Chem. 31 (4) (1972) 577–638, https://doi.org/10.1351/pac197231040577.
[28] D. Brühwiler, H. Frei, J. Phys. Chem. B 107 (2003) 8547–8556.
[29] D. Zhao, Q. Huo, J. Feng, B.F. Chmelka, G.D. Stucky, J. Am. Chem. Soc. 120 (1998) 6024–6036.
[30] D.W. Marquardt, J. Soc. Ind. Appl. Math. 11 (1963) 431–441.
[31] The Levenberg-Marquardt method implemented in Mathcad 14, Mathsoft Eng. & Edu., Inc. (http://www.mathsoft.com).
[32] M. Kruk, M. Jaroniec, Chem. Mater. 15 (2003) 2942–2949.
[33] A.L. Myers, AlChE J 29 (4) (1983) 691–693.
[34] a) R.G. Jordi, D.D. Do, J. Chem. Soc. Faraday. Trans. 88 (16) (1992) 2411–2419;
b) A. Micke, M. Billow, M. Kocirik, P. Struve, J. Phys. Chem. 98 (1994) 12337–12344.c)P. M. Mathias, R. Kumar, J. D. Moyer, Jr., J. M. Schork, S. R. Srinivasan, S. R. Auvil, O. Talu, Ind. Eng. Chem. Res. 351 (996) 2477-2483.
[35] a) L. Song, L.V.C. Rees, J. Chem. Soc. Faraday. Trans. 93 (4) (1997) 649–657;
b) W. Zhu, F. Kapteijn, J.A. Moulijn, Chem. Commun. (1999) 2453–2454;
c) T.J.H. Vlugt, R. Krishna, B. Smit, J. Phys. Chem. B 103 (1999) 1102–1118;
d) R. Krishna, T.J.H. Vlugt, B. Smit, Chem. Eng. Sci. 54 (1999) 1751–1757.
[36] a) D. Paschek, R. Krishna, Phys. Chem. Chem. Phys. 2 (2000) 2389–2394;
b) W. Zhu, F. Kapteijn, J.A. Moulijn, M.C. den Exter, J.C. Jansen, Langmuir 16 (2000) 3322–3329.
[37] a) S. Keskin, J. Liu, J.K. Johnson, D.S. Sholl, Langmuir 24 (2008) 8254–8261;
b) J.A. Ritter, S.J. Bhadra, A.D. Ebner, Langmuir 27 (2011) 4700–4712;
c) S.J. Bhadra, A.D. Ebner, J.A. Ritter, Langmuir 28 (2012) 6935–6941.
[38] a) S. García, J.J. Pis, F. Rubiera, C. Pevida, Langmuir 29 (2013) 6042–6052;
b) K. Liu, B. Li, Y. Li, X. Li, F. Yang, G. Zeng, Y. Peng, Z. Zhang, G. Li, Z. Shi, S. Feng, D. Song, Chem. Commun. 50 (2014) 5031–5033;
c) A. Farzaneh, M. Zhou, E. Potapova, Z. Bacsik, L. Ohlin, A. Holmgren, J. Hedlund, M. Grahn, Langmuir 31 (2015) 4887–4894.
[39] T. Suzuki, M. Hirano, H. Tamon, M. Okazaki, J. Phys. Chem. 99 (1995) 15968–15972.
[40] a) G. Calzaferri, Phys. Chem. Chem. Phys. 20 (2018) 29070–29084;
b) G. Calzaferri, Phys. Chem. Chem. Phys. 19 (2017) 10611–10621.
[41] The value of the equation (14) is very sensitive to n only for small cavities, $n<80$, but can be larger for significantly larger cavities as present in SBA-15, for which $n = 235$ must be used. for a discussion see [7].
[42] P.W. Atkins, J. de Paula, Physikalische Chemie, vol. 4, Wiley-VCH Weinheim, Auflage, 2006. ISBN 3-527-31546-2.
[43] A. Galarneau, H. Cambon, F. Di Renzo, F. Fajula, Langmuir 17 (2001) 8328–8335.
[44] V.-T. Hoang, Q. Huang, M. Eić, T.-O. Do, S. Kaliaguine, Langmuir 21 (2005) 2051–2057.
[45] M. Kruk, M. Jaroniec, C.H. Ko, R. Ryoo, Chem. Mater. 12 (2000) 1961–1968.
[46] A. Sayari, Y. Yang, Chem. Mater. 17 (2005) 6108–6113.